

5-1-2013

Dissolution Rates of Amorphous Al- and Fe-Phosphates and their Relevance to Phosphate Mobility on Mars

Valerie Tu

University of Nevada, Las Vegas, valerie.chavez@gmail.com

Follow this and additional works at: <https://digitalscholarship.unlv.edu/thesesdissertations>

 Part of the [Astrophysics and Astronomy Commons](#), [Geochemistry Commons](#), and the [Geology Commons](#)

Repository Citation

Tu, Valerie, "Dissolution Rates of Amorphous Al- and Fe-Phosphates and their Relevance to Phosphate Mobility on Mars" (2013). *UNLV Theses, Dissertations, Professional Papers, and Capstones*. 1900.
<https://digitalscholarship.unlv.edu/thesesdissertations/1900>

This Thesis is brought to you for free and open access by Digital Scholarship@UNLV. It has been accepted for inclusion in UNLV Theses, Dissertations, Professional Papers, and Capstones by an authorized administrator of Digital Scholarship@UNLV. For more information, please contact digitalscholarship@unlv.edu.

DISSOLUTION RATES OF AMORPHOUS AL- AND FE-PHOSPHATES AND
THEIR RELEVANCE TO PHOSPHATE MOBILITY ON MARS

By

Valerie M. Tu

Bachelor of Science in Geology
University of Nevada, Las Vegas
2011

A thesis submitted in partial fulfillment
of the requirements for the

Master of Science in Geoscience

Department of Geoscience
College of Science
The Graduate College

University of Nevada, Las Vegas
May 2013

Copyright by Valerie M. Tu, 2013
All Rights Reserved



THE GRADUATE COLLEGE

We recommend the thesis prepared under our supervision by

Valerie Tu

entitled

Dissolution Rates of Amorphous Al- and Fe-Phosphates and their Relevance to Phosphate Mobility on Mars

be accepted in partial fulfillment of the requirements for the degree of

Master of Science in Geoscience

Department of Geoscience

Elisabeth Hausrath, Ph.D., Committee Chair

Scott Nowicki, Ph.D., Committee Member

Eugene Smith, Ph.D., Committee Member

Gary Cerefice, Ph.D., Graduate College Representative

Tom Piechota, Ph.D., Interim Vice President for Research &
Dean of the Graduate College

May 2013

Abstract

Dissolution Rates of Amorphous Al- and Fe-Phosphates and their Relevance to Phosphate Mobility on Mars

Tu, V.

Keywords: phosphate, weathering, astrobiology, Mars, soils

Phosphate is an essential element for life on Earth, and therefore if life exists or ever existed on Mars it may have required phosphate. Amorphous Al- and Fe-phosphates rapidly precipitate from acidic solutions and amorphous Al-phosphates likely control phosphate concentrations in some natural waters on Earth. Amorphous phases may be even more important on Mars than on Earth, and amorphous phosphates are therefore likely important in the phosphate cycle on Mars. Despite this importance, however, few dissolution rates exist for amorphous Al- and Fe- phosphates. In this study, dissolution rates of amorphous Al- and Fe-phosphates were measured in flow-through reactors from steady state concentrations of Al, Fe and P. A pH –dependent rate law was calculated from the dissolution rates $\log R = \log k - npH$, where R is the dissolution rate, k is intrinsic rate constant and n is the rate dependence on pH. For amorphous Al-phosphate, $\log k = -6.539 \pm 1.529$, and $n = 2.391 \pm 0.493$. For amorphous Fe-phosphate, $\log k = -13.031 \pm 0.558$, and $n = 1.376 \pm 0.221$. Amorphous Al-phosphate dissolves stoichiometrically under all conditions, and amorphous Fe-phosphate dissolves non-stoichiometrically, approaching stoichiometric dissolution as pH decreases, due potentially to Fe-oxides precipitating and armoring grain surfaces. Perhaps due to these effects, amorphous Al-phosphate dissolution rates are approximately three orders of magnitude faster than amorphous Fe-phosphate dissolution rates. Amorphous Al-

phosphate dissolution rates measured in this study are also faster than published variscite dissolution rates. Dissolution rates of amorphous Al- and Fe-phosphates in this study therefore imply rapid phosphate release into acidic environments, suggesting phosphate mobility under Mars-relevant conditions.

Acknowledgments

I would like to express my very sincere gratitude to all of the individuals who helped me along my journey, first and foremost I would like to express my gratitude to my advisor Dr. Elisabeth Hausrath for her patience, encouragement and guidance, she is no doubt a remarkable woman and I'm very fortunate to have learned so much from her.

Special thanks go to Dr. Eugene Smith, and Dr. Scott Nowicki, for not just being my committee members but also for playing an important part in my education and experiences, I am very fortunate to have been taught by you both. Also, a very special thanks to Dr. Gary Cerefice, my thesis committee member, I thank you for your invaluable contribution you spent reviewing this thesis and helping me to better improve upon my project.

I am truly grateful to the following individuals for all their contributions and support over the years: Seth Gainey, Christopher Adcock, Michael Steiner, Renee Schofield, Fritz Freudenberger, Kirellos Sefein, Brittany Meyers, and Julie Baumeister thank you for all of your support and help. I would also like to acknowledge Oliver Tschauner, Paul Forster, Rachael Johnsen, Brandon Guttery and Mingua Ren for their contributions to this project. I would especially like to acknowledge my family: my step-sons Nicholas and Tyler, my mom Helen-Sofie, dad Steven, sister Samantha, and brother Raymond- thank you all so much for your love and support and to my loving husband, Vincent Tu, thank you for caring for our children, supporting me and allowing me to pursuit a better future for our family.

We would like to acknowledge funding from the Mars Fundamental Research Program Grant NNX10AP58G to E. M. Hausrath, Marathon Oil Corporation, the Hispanic Scholarship Fund, the UNLV Geoscience Department, and the Graduate and Professional Students Association.

Dedication

I would like to dedicate this thesis to my son Kaede who no doubt has had to endure much sacrifice without his mom around when these studies were carried out. This thesis is dedicated to YOU sweetheart!

Table of contents

ABSTRACT.....	iii
ACKNOWLEDGEMENTS.....	v
DEDICATION.....	vii
LIST OF TABLES.....	x
LISTS OF FIGURES.....	xii
Chapter 1 Introduction.....	1
Chapter 2 Methods	
Materials.....	4
Experimental Set-up.....	5
Analyses.....	6
Chapter 3 Calculations	
Dissolution rate calculation.....	8
Rate laws.....	8
Chapter 4 Saturation indices.....	10
Chapter 5 Results	
Solution pH.....	11
Concentrations.....	11
Stoichiometry of Release.....	11
Saturation state of minerals.....	11
Reacted Material Characterization.....	12
Chapter 6 Discussion.....	13
Chapter 7 Implications for Mars.....	17

Chapter 8 Conclusions.....	18
Appendix A	
Appendix A Figure captions.....	19
Appendix A Tables.....	22
Appendix A Figures.....	27
Appendix B	
Appendix B Tables.....	35
Appendix B Figures.....	52
References.....	72
Curriculum Vitae.....	76

List of Tables

Table 1 Summary of experimental conditions for the dissolution of amorphous Al-phosphates.....22

Table 2 Summary of experimental conditions for the dissolution of amorphous Fe-phosphates.....23

Table 3 Mineral solubility constants.....24

Table 4 Saturation indices for the average of each steady state condition.....25

Table 5 Saturation indices for the average of each steady state condition.....26

Table 1B Dissolution results from pH 3 amorphous Fe-phosphate experiment.....35

Table 2B Dissolution results from pH 2.5 amorphous Fe-phosphate experiment.....36

Table 3B Dissolution results from pH 2 amorphous Fe-phosphate experiment.....37

Table 4B Dissolution results from pH 1 amorphous Fe-phosphate experiment.....38

Table 5B Dissolution results from pH 3 amorphous Al-phosphate experiment.....39

Table 6B Dissolution results from pH 2.5 amorphous Al-phosphate experiment.....40

Table 7B Dissolution results from pH 2 amorphous Al-phosphate experiment.....41

Table 8B Dissolution results from pH 1 amorphous Al-phosphate experiment.....	42
Table 9B Results of Amorphous Fe-phosphate pH 1 PHREEQ-C solubility determination.....	43
Table 10B Results of Amorphous Fe-phosphate pH 2 PHREEQ-C solubility determination.....	44
Table 11B Results of Amorphous Fe-phosphate pH 2.5 PHREEQ-C solubility determination.....	45
Table 12B Results of Amorphous Fe-phosphate pH 3 PHREEQ-C solubility determination.....	46
Table 13B Results of Amorphous Al-phosphate pH 1 PHREEQ-C solubility determination.....	47
Table 14B Results of Amorphous Al-phosphate pH 2 PHREEQ-C solubility determination.....	48
Table 15B Results of Amorphous Al-phosphate pH 2.5 PHREEQ-C solubility determination.....	49
Table 16B Results of Amorphous Al-phosphate pH 3 PHREEQ-C solubility determination.....	50
Table 17B Solution results from pH 2.5 amorphous Al-phosphate batch experiment and amorphous Fe-phosphate stopped flow-through/reactor experiment.....	51

List of Figures

Appendix A, Figure 1.	27
Appendix A, Figure 2.	28
Appendix A, Figure 3.....	29
Appendix A, Figure 4.....	30
Appendix A, Figure 5.....	31
Appendix A, Figure 6.....	32
Appendix A, Figure 7.....	33
Appendix A, Figure 8.....	34
Appendix B, Figure 1.....	52
Appendix B, Figure 2.....	53
Appendix B, Figure 3.....	54
Appendix B, Figure 4.....	55
Appendix B, Figure 5.....	56
Appendix B, Figure 6.....	57
Appendix B, Figure 7.....	58
Appendix B, Figure 8.....	59
Appendix B, Figure 9.....	60
Appendix B, Figure 10.....	61
Appendix B, Figure 11.....	62
Appendix B, Figure 12.....	63
Appendix B, Figure 13.....	64
Appendix B, Figure 14.....	65

Appendix B, Figure 15.....	66
Appendix B, Figure 16.....	67
Appendix B, Figure 17.....	68
Appendix B, Figure 18.....	69
Appendix B, Figure 19.....	70
Appendix B, Figure 20.....	71

Chapter 1 Introduction

Due to its importance to habitability and the aqueous history of Mars, multiple studies have examined phosphate on Mars. High phosphorus content in Martian soils is thought to be the product of acidic weathering of igneous rock [Greenwood, 2006]. Soluble phosphates have been identified by the Mars Exploration Rover, Opportunity, in outcrops at Eagle Crater on Mars [Rieder, 2004]. Dreibus et al. [1996] demonstrated that acidic fluids easily dissolved phosphates from SNC meteorites. Previous work by Ming et al. [2006], have proposed that P may occur in Ca-, Fe- and Al- phases on Mars based on Alpha Particle X-ray Spectrometer (APXS) and Mossbauer Spectrometer results. Tosca et al. [2004] indicate the presence of an Fe- phosphate phase in acidic Mars-analog experiments and Ruff et al. [2006] suggest that an Al-phosphate phase, wavellite, may be present in the Martian rock Watchtower. Lane et al [2008] have proposed that ferristrunzite and/or strengite are present in Paso Robles soil, and Hausrath et al. [2013] suggested that a ferric phosphate such as ferrian giniite may be present in Paso Robles soil based on laboratory experiments and Mössbauer measurements. The lack of correlation between phosphorous concentrations and nanophase oxides in dusts measured by the Mars Exploration Rovers indicate that sorbed phosphate may not be the dominant phase in Martian soils [Morris et al., 2006], although other work suggests sorbed phosphates may be present [Barger-Rampe and Morris, 2012]. Therefore, despite their importance, phosphates remain poorly understood on Mars.

Increasing evidence suggests the importance of amorphous phases on Mars. Amorphous weathering products, such as allophane, amorphous silica, and palagonite

have been detected by orbital mid-infrared and *in-situ* mineralogical and chemical analyses [Michalski, 2005; Barger-Rampe and Morris, 2012]. *In situ* measurements at Meridiani Planum indicate spectra consistent with opaline silica [Wray, 2012] and rocks within the Meridiani sulfate-bearing terrain contain amorphous silica [Clark et al., 2005; Glotch et al., 2006]. The CheMin instrument aboard the Mars Science Laboratory (MSL) has successfully identified amorphous phases at Rocknest, likely either basaltic glass, previously detected at Columbia Hills [Ruff, 2006] or weathered basalt, similar to weathered basalts in Hawaii [Bish, 2012]. Under the water-limited conditions likely present on Mars, amorphous phases are likely to be important [Tosca et al., 2009].

Roncal-Herrero et al. [2009] report that the first phosphate-containing phases to precipitate from super-saturated acidic fluids in laboratory experiments are amorphous Al- and Fe-phosphates. In long term (up to 5 years) laboratory experiments designed to test whether amorphous phosphates eventually become variscite after prolonged aging, Hsu [1982a] concluded that amorphous Al-phosphates, not variscite, are the likely products of phosphate fertilizers in acidic terrestrial soils. Similar long-term aging experiments of amorphous Fe-phosphates indicated that they were unlikely to recrystallize to strengite for up to 66 months [Hsu 1982b]. Analyses of terrestrial natural waters indicate that Al and phosphate concentrations are consistent with control by equilibrium with either variscite or amorphous Al-phosphate under acidic conditions [Roncal-Herrero and Oelkers 2011], and sequential-fractionation data from extraction analyses of cultivated sandy soils from citrus groves in Florida suggest that amorphous Al- and Fe-phosphates and P associated with crystalline Al- and Fe-oxides account for a significant portion of the total P [Zhang et al., 2001]. Due to the likely prevalence of

amorphous phases on Mars [Tosca et al., 2004], and the rapid formation and long persistence of amorphous Al- and Fe-phosphates on Earth, amorphous Al- and Fe-phosphate phases are likely important phosphate sources in weathering environments on Mars.

Despite their potential importance, however, few experiments have examined the dissolution rates of and phosphate release from amorphous phosphate-containing phases [Huffman, 1960]. In this study, we measure the dissolution rates of and phosphate release from amorphous Al- and Fe- phosphates, to shed light on phosphate mobility on Mars.

Chapter 2 Methods

Materials

Amorphous Al- and Fe-phosphates were synthesized in batch reactors after Roncal-Herrero et al. [2009], except that syntheses were performed at 50°C for 24 hours, continuously shaken at 100 strokes per minute and larger volumes were used to yield sufficient mass for dissolution experiments. Materials were synthesized, ensuring reproducible, pure phases for use in baseline dissolution experiments. Syntheses were performed for 12, 24, and 48 hour durations and a 24-hour synthesis was chosen because particles had coalesced to a more solid mass (Appendix B Figures 19a-c and Figures 20a-c), but no evidence of crystallinity was detected (Appendix A Figures 8a-b). In all cases, solutions were made with 18.2 M Ω deionized water and high purity chemicals. Aqueous solutions (0.1M Al- or Fe-(NO₃)₃), and 0.1M KH₂PO₄ and 0.09M KOH) were preheated to 50°C, combined while continuously stirring and immediately sealed and immersed in the 50°C shaking water bath. Batches were cooled to 25° C after 24 hours, and the slurry centrifuged at 11.5 rad for 2-10 minutes until supernatants were clear. Supernatants were decanted, and solid phases washed 3 times with 18.2 M Ω deionized water and air dried at room temperature for 2-5 days. Powders were analyzed by X-ray diffraction (XRD) and indicate amorphous material. Analyses were completed using a PANalytical X'PERT Pro X-ray Diffraction Spectrometer and Cu Kα radiation ($\lambda = 1.5406 \text{ \AA}$) with data collected every 0.02 degrees 2θ at 20 mA and 40kV from 5 to 75 degrees 2θ with a step size of 0.08° in the X-ray Diffraction and X-ray Fluorescence Laboratory (XXL) at UNLV, (Appendix A Figures 8a-b). Powdered samples were gold coated and observed using a JEOL JSM-6700F Field Emission Scanning Electron Microscope (FE-SEM) at

working distances of 8.0mm to 8.4mm at 2.0 or 5.0kV in Secondary Electron Imaging mode (SEI) and a Scanning Electron Microscope (SEM) (JEOL ASM-5600), at a working distance of 20mm and accelerating voltage of 15kV, with a spot-size of 20 and using Energy Dispersive Spectroscopy (EDS) for composition determination in the Electron Microanalysis and Imaging Laboratory (EMIL) at UNLV. Surface areas were determined using a Micromeritics ASAP 2020 Gas Sorption Analyzer using N₂ and are 121.9128 ± 0.4702 (m²/g) (amorphous Fe-phosphate) and 77.155 ± 0.3943 (m²/g) (amorphous Al-phosphate).

Experimental Set-up

In order to determine dissolution rates under Mars-relevant acidic conditions, dissolution experiments of amorphous Al- and Fe-phosphates at pH values of 1, 2, 2.5 and 3 were conducted using flow-through reactors based on those used by Weissbart and Rimstidt [2000] (Appendix A, Figure 1). Samples were sieved to 75-150μm particle size, and 1.000 to 3.000 ± 0.004 g was placed on a 0.45μm acrylic membrane filter held in place with an acrylic sleeve within the reactor, with the reactor already filled with solution to prevent the formation of bubbles. The input solution consisted of a 0.01M KNO₃ solution adjusted to the pH of the experiment (1, 2, 2.5, or 3) with high purity 1 N HCl and 1 N NaOH. Solution was pumped up through the filter using a VWR variable-speed ultra low-flow peristaltic feed pump, and the reactor was continuously agitated on a shaker plate at 150 rpm. Uncertainty on flow-rates for pump 1 is ± 0.029 ml/min and for pump 2 is ± 0.048 ml/min. The outlet solution was filtered through a 0.45μm filter before entering the collection vessel, and concentrations were measured until steady state was obtained, defined as at least four consecutive data points

of pH values that do not vary more than ± 0.1 units, flow rates that do not vary more than ± 0.05 ml/min, and concentrations that do not vary by more than 10%. In one experiment (pH = 2.5), the reactor was perturbed, affecting the phosphate concentrations (Appendix B Figure 3D). Steady state concentrations at saturation of Fe, Al and P were also measured either in a batch reactor (Al-phosphate) or a flow-through reactor with the flow rate stopped (Fe-phosphate) after ~ 2 weeks (Appendix B table 17B).

Analyses

Outlet solutions were collected at predetermined intervals based on preliminary experiments, weighed for flow rate determination, and measured for pH using a SevenEasy Mettler Toledo AG pH probe. Separate aliquots were re-filtered through $0.45\mu\text{m}$ filters, acidified to below pH 2 using 1 N high purity HCl for preservation, and stored at 4°C until chemical analysis.

Aluminum concentrations were measured by the catechol violet colorimetric method [Dougan and Wilson, 1974] at a wavelength of 585 nm, and phosphate concentrations were determined by the molybdate blue colorimetric method [Murphy and Riley, 1962] at a wavelength of 882 nm on a Thermo Scientific Genesys 10S UV-Vis Spectrophotometer. Flame atomic absorption spectroscopy (AAS) was used to measure Fe concentrations on a Thermo Scientific iCE 3000 series AA spectrometer. The uncertainty on instrumentation for analysis is as follows, for Fe concentrations the uncertainty is ± 0.0164 ppm [Perkin-Elmer, 1964], and for Al and P (as phosphate) ± 0.0435 ppm. The method uncertainty is documented as ± 0.19 ppm for Fe [Greenberg et al., 2005], Al $\pm 2\%$ Dougan and Wilson [1974], and P (as phosphate) is $\pm 8\%$ Murphy and Riley [1962]. Uncertainty on analyses was estimated by repeated measurements of

standards and blanks, based on modified methods by [Perkin-Elmer, 1964], and was determined to be one standard deviation.

Chapter 3 Calculations

Dissolution rate calculation

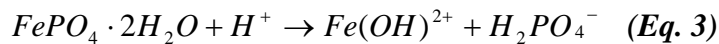
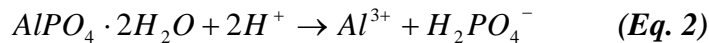
Dissolution rates were calculated from steady state Al, Fe and P concentrations and flow rates normalized to BET surface area [White and Brantley, 1995]:

$$R = \frac{(C_{out} - C_{in})Q}{A \cdot m} \quad (\text{Eq. 1})$$

where C_{out} is the measured steady state output concentration (mM), C_{in} is the input concentration (mM) (assumed to be zero based on below detection measurements of all method blanks), Q is the flow rate (L/s), A is the specific surface area (cm^2/g), and m is the mass (g). Rates were normalized to final, assumed to be steady state, masses, multiplied by the specific surface area.

Rate laws

Rate laws were established for amorphous Al- and Fe-phosphate dissolution by applying linear regression analysis to the log dissolution rates versus pH values from each experiment. The pH dependence of dissolution of amorphous Al- and Fe-phosphate is fit to the following equation: $\log R = \log k - npH$, where R is the dissolution rate, k is the intrinsic rate constant and n is the rate dependence on pH. For amorphous Al-phosphate, $\log k = -6.539 \pm 1.529$, and $n = 2.391 \pm 0.493$. For amorphous Fe-phosphate, $\log k = -13.031 \pm 0.558$, and $n = 1.376 \pm 0.221$. The larger reaction order with respect to H^+ for Al versus Fe, is consistent with the following dissolution equations:



Values were calculated based on a range of 3 pH values in our experiments, 2, 2.5 and 3

because the material had completely dissolved in the pH1 experiment (Appendix A, Figure 5).

Chapter 4 Saturation indices

Saturation indices were calculated for each steady state condition using PhreeqC [Parkhurst and Appelo, 1999], for strengite, variscite, goethite, hematite, maghemite, vivianite, ferrihydrite, 10nm goethite, 10nm maghemite, 10nm hematite, and gibbsite using values from [Parkhurst and Appelo, 1999; Elwood-Madden et al., 2009; Roncal-Herrero and Oelkers, 2011] (Appendix A, Table 3). Due to the uncertainties in the solubilities of amorphous Al- and Fe-phosphates [Roncal-Herrero and Oelkers, 2011] saturation indices were not calculated for the amorphous Al- and Fe-phosphates. However, our stopped-flow and batch experiments, which show higher concentrations than the steady state concentrations from our flow through reactors at the same pH, indicate that the experimental conditions are undersaturated with respect to these phases.

Chapter 5 Results

Solution pH

Output solution pH values typically displayed one of two behaviors, either displaying constant pH values throughout the experiment, or increasing from low initial pH values to steady state values (Appendix A Figure 2B, Appendix A Tables 1-2, and Appendix B Figures 1B-8B).

Concentrations

Fe and Al concentrations typically display one of two behaviors, either remaining steady throughout the entire experiment, or decreasing from initially higher concentrations to reach steady values (Appendix A Figure 2C-D, Appendix A Tables 1-2, Appendix B Figures 1C-8C, and Appendix B Tables 1B-8B). Phosphorus concentrations generally decreased over time in all experiments (Appendix A Figure 2D, Appendix A Tables 1-2, Appendix Figures B 1D-8D and Appendix B Tables 1B-8B).

Stoichiometry of Release

Dissolution of amorphous Fe-phosphate was non-stoichiometric in all cases, but approached stoichiometric dissolution as pH decreased (Appendix A Figure 3). In contrast, amorphous Al-phosphate dissolution was stoichiometric in all experiments (Appendix A Figure 4). The fluctuation in non-stoichiometric dissolution observed in the pH = 2.5 experiment is attributed to the perturbation of the reactor during this period of time.

Saturation state of minerals

Saturation indices determined using PhreeqC [Parkhurst and Appelo, 1999] were undersaturated with respect to all Fe-bearing secondary phases tested (Appendix A

Tables 3-5). Saturation indices for Al-phosphate experiments indicate that solutions are undersaturated with respect to gibbsite, and over-saturated with respect to variscite (crystalline Al-phosphate), which is not surprising for dissolution of an amorphous phase.

Reacted Material Characterization

Reacted and unreacted amorphous Al- and Fe-phosphates were imaged by FE-SEM and indicate a decrease in the size of the globules (Appendix A Figures 6a-d and 7a-d) after reaction. Unreacted amorphous Al-phosphate has globule sizes of ~ 45 to 64nm in diameter, and unreacted amorphous Fe-phosphate globule sizes of ~ 26 to 100nm in diameter. Reacted amorphous Al-phosphate material demonstrates slightly smaller diameters than that of unreacted material (~ 27 to 33 nm) (Appendix A Figures 6a-c), and no apparent difference was observed in the size of the reacted Fe-phosphate globules.

Chapter 6 Discussion

The dissolution rates measured in this study indicate that amorphous Al-phosphates dissolve more rapidly than the crystalline Al-phosphate variscite (Appendix A Figure 5). This result is similar to previous studies, which indicate that amorphous silica, for example, dissolves more rapidly than quartz [Liang and Readey, 1987]. Amorphous Fe-phosphate dissolution rates from this study were compared to dissolution rates of crystalline and colloidal Fe-phosphates from the literature [Huffman, 1960]. Our dissolution rates at pH 2, 2.5, and 3 are slower than the dissolution rates reported at pH 6 (Appendix A Figure 5), although since dissolution rates for strengite and colloidal Fe phosphate were not reported for similar experimental conditions at similar pH values, rates cannot be directly compared. Aqueous solutions interacting with amorphous phases are therefore likely to release more phosphate than is released from aqueous interactions with crystalline phosphate phases.

The amorphous Al- and Fe-phosphates used in this study are quite similar. The unreacted amorphous Al- and Fe-phosphates used in this study have similar large surface areas (although the surface area of the Fe phosphate is approximately one and one half times greater than the surface area of Al phosphate), and both consist of nanoporous material as observed by FE-SEM (Appendix A Figures 6a-d and 7a-d, and Appendix B Figures 10-20). In addition, although we did not synthesize solid solutions of amorphous Al- and Fe- phosphates, many Al and ferric phosphate phases have complete solid solution including strengite and variscite [Huminicki and Hawthorne, 2002; Taxer and Bartl, 2004] . Despite the similarities between the amorphous phases, however, the dissolution rates measured here are much slower for the amorphous Fe-

phosphates than for amorphous Al-phosphates (Appendix A Figure 5). This result is similar to previous results indicating that strengite dissolves more slowly than variscite at comparable citrate concentrations and pH, with the effect decreasing with increased pH [Malunda, 2000]. Perhaps explaining the difference in dissolution rates between the phases, the dissolution of amorphous Al-phosphate is stoichiometric, whereas the dissolution of the amorphous Fe phosphate is non-stoichiometric (Appendix A Figures 3 and 4).

Non-stoichiometric dissolution can be due to a number of causes. Common mechanisms identified in the literature consist of the formation of a leached layer, grinding or re-precipitation. Chin and Mills [1991] observed in acidic kaolinite dissolution experiments that sorption and precipitation of silica might cause incongruent dissolution. Cubillas et al. [2005] observed a mineral coating of otavite on CaCO_3 in near neutral dissolution experiments, which decreased dissolution rates. Hellmann et al. [2003] proposed an interfacial dissolution-re-precipitation mechanism in labradorite feldspar experiments. Weissbart and Rimstidt [2000] documented, in wollastonite dissolution experiments aimed at improving models of leached layer formation, the formation of a hydrated silica leached layer influencing the dissolution of wollastonite in solutions with pH ranging from 2 to 6. Putnis [2009] proposed an interface-coupled dissolution precipitation reaction for a variety of minerals including quartz, kaolinite and feldspar. Ruiz-Agudo et al. [2012] utilized Putnis' mechanism in reporting evidence that an amorphous silica leached layer is formed via a tight interface-coupled two-step process: stoichiometric dissolution of mineral surfaces and subsequent precipitation of a

secondary phase from a supersaturated boundary layer of fluid in contact with the mineral surface.

In dissolution experiments of Fe-bearing minerals that may be particularly relevant to dissolution of the amorphous Fe-phosphates in our study, $\text{Fe}(\text{OH})_3$ precipitation may be the controlling factor causing incongruent dissolution. Elwood Madden et al. [2012] observed incongruent jarosite dissolution thought to be dependent on iron(hydr)oxide reaction products formed in solutions at $\text{pH} > 3.5$. Siever and Woodford [1979] described the development of a precipitated $\text{Fe}(\text{OH})_3$ layer, armoring mafic mineral surfaces such as fayalite, hypersthene, basalt and obsidian. Huffman et al. [1960] report incongruent dissolution of strengite and colloidal ferric phosphate in water, similar to our findings. Huffman et al. [1960] also indicate surface coatings on strengite and colloidal ferric phosphate of ferric-hydroxide, which they confirm by microscopic examination. Malunda [2000] also observed non-stoichiometric dissolution of strengite, which they attributed to the formation of a secondary phase or a surface complex of Fe. In Al- and Fe-phosphate precipitation experiments, Hsu [1976] demonstrated rapid formation of Fe-oxides, which they attribute to the much larger first hydrolysis constant for Fe^{3+} of (2.5×10^{-3}) [Lamb and Jacques, 1938], compared to the first hydrolysis constant of Al^{3+} (1.05×10^{-5}) [Frink and Peech, 1963]. We therefore postulate that the non-stoichiometric dissolution of amorphous Fe-phosphate and the slow dissolution rates relative to amorphous Al-phosphate observed in these experiments may be due to the re-precipitation of secondary Fe-oxide phases. These findings are similar to the findings of Huffman [1960], Siever and Woodford [1979], and Elwood-Madden et al. [2012], due to the much larger first hydrolysis constant for Fe^{3+} than for Al^{3+} .

In order to investigate the possible formation of Fe-oxy(hydr)oxides, the saturation state of our output solutions was calculated relative to strengite, goethite, hematite, maghemite, vivianite, ferrihydrite, 10nm goethite, 10nm hematite, and 10nm maghemite [Parkhurst and Appelo, 1999; Roncal-Herrero and Oelkers, 2011; Elwood-Madden et al., 2012] (Appendix A Table 4), and was found to be undersaturated with respect to all of these minerals. This result is consistent with the results of Ruiz-Agudo et al., [2012], who document the formation of a re-precipitated secondary phase using *in situ* atomic force microscopy (AFM) and FE-SEM despite undersaturation of the bulk solution with respect to secondary phases.

Amorphous phases are likely important on Mars [Tosca, 2004; Michalski, 2005; Barger-Rampe and Morris, 2012; Wray, 2012], amorphous Al- and Fe-phosphates are likely important on Earth [Hsu, 1982a, b; Roncal-Herreo and Oelkers, 2011], and the measurement of their dissolution rates yields important information about potential phosphate mobility on Mars and on Earth. Dissolution rates were measured in flow through reactors, which although complicated to run, yield the most easily interpreted data. In this case, an additional possibility is the transport of suspended phases. Although images of unreacted and reacted phases show decreased globular sizes, indicative of surface dissolution of the agglomerated particle, previous work on natural waters has shown significant transport of trace elements in the colloidal fraction [Dupre et al., 1996; Viers et al., 1997]. Therefore, transport of colloidal particles may be an important process under very acidic conditions on Mars, similar to acid rock drainage on Earth, yielding increased transport and dissolution such as is observed for spalling glass surfaces in dissolution experiments on Earth [Gislason and Oelkers, 2003].

Chapter 7 Implications for Mars

Mars is more P-rich than Earth [Filippelli, 2008] and likely to have amorphous phases [Michalski, 2005; Ruff, 2006; Bish 2008; Tosca, 2009; Barger-Rampe and Morris, 2012; Wray, 2012]. Phosphate is an essential nutrient for life [Wald, 1964] and is important for determining habitability on Mars. We conclude from these studies that amorphous phosphates are likely to release more phosphate than crystalline phases, suggesting more abundant phosphate in Martian environments. Results from the dissolution of amorphous Al- and Fe-phosphates can also be utilized for future modeling and predictions of phosphate mobility on Mars.

Chapter 8 Conclusions

Phosphate is an essential nutrient for life and amorphous Al- and Fe-phosphates are likely important in controlling phosphate concentrations and phosphate mobility on Mars. Phosphates have been identified within martian soils, rocks and meteorites. Amorphous phases have been identified on Mars and recent data and observations from MSL suggest amorphous phases may be abundant. Few dissolution rates for amorphous Al- and Fe-phosphates exist in the literature and therefore, determination of dissolution rates and rate laws are critical to understanding phosphate concentrations on Mars.

Dissolution rates for amorphous Al- and Fe-phosphates have been determined in acidic flow-through dissolution experiments. Amorphous Al-phosphate yields congruent dissolution rates that are faster than its crystalline counterpart, variscite, and than amorphous Fe-phosphate. Reacted amorphous Al-phosphate contains smaller globules than the unreacted material, indicative of dissolution. In contrast, the amorphous Fe-phosphate dissolved incongruently and more slowly than the amorphous Al-phosphate, which may be due to the re-precipitation of Fe-oxides, armoring grain surfaces, and inhibiting dissolution. Rate laws of the form $\log R = \log k - npH$ were calculated from dissolution rates, with values for amorphous Al-phosphate of: $\log k = -6.539 \pm 1.529$, and $n = 2.391 \pm 0.493$ and amorphous Fe-phosphate, $\log k = -13.031 \pm 0.558$, and $n = 1.376 \pm 0.221$. The fast dissolution rates of amorphous Al- and Fe-phosphates indicate rapid release of phosphates into acidic environments, such as those potentially on Mars, suggesting enhanced phosphate mobility on that planet.

Appendix A Figure Captions

Appendix A, Figure 1. (A) Schematic image of flow-through reactor based on Weissbart and Rimstidt (2008). Solution is pumped from the input reservoir using a peristaltic pump up through a 0.45 micron filter. The reactor is agitated atop a shaker plate at 150 rpm, and then solution is filtered (0.45 μm filter) before entering a collection vessel for analyses. (B) Enlarged schematic image of reactor showing flow of fluid up through sample suspended on the filter. The filter is being held in place by an acrylic sleeve and effluent solution flowing out is filtered before being collected in a vessel for analyses.

Appendix A, Figure 2. Representative results of dissolution of amorphous Al-phosphate (pH 2.5) (A) Flow rate (mol/min), (B) output pH (C). Al (mM) and (D) P (mM) versus time. Boxes indicate steady state conditions defined as described in text.

Appendix A, Figure 3. Aqueous Fe: P ratio (mM) for each dissolution experiment of amorphous Fe-phosphate (A) pH = 3 (B) pH = 2.5 (C) pH = 2 and (D) pH = 1. The solid horizontal line represents the ratio of Fe: P in the amorphous Fe phosphate. Results indicate non-stoichiometric dissolution of amorphous Fe-phosphate at higher pH with concentrations approaching stoichiometric release as pH decreases.

Appendix A, Figure 4. Aqueous Al: P ratio (mM) for each dissolution experiment of amorphous Al-phosphate at (A) pH = 3 (B) pH = 2.5 (C) pH = 2 and (D) pH = 1. The solid horizontal line represents the ratio of Al: P in the amorphous Al phosphate. Results indicate non-stoichiometric dissolution of amorphous Al-phosphate initially, which in all cases achieve stoichiometric dissolution by steady state conditions.

Appendix A, Figure 5- Dissolution rates of amorphous Al- and Fe-phosphates versus pH indicate that Al-phosphates dissolve more rapidly than amorphous Fe-phosphates, which may be due to re-precipitation of Fe oxides. Amorphous Al-phosphates measured in this study are also faster than the crystalline Al phosphate variscite. Lines represent the rate laws calculated as described in the text.

Appendix A, Figure 6- Micrographs of nanoporous amorphous Al-phosphate taken by Field-Emission Scanning Electron Microscopy (FE-SEM). A) 24 hour synthesized amorphous Al-phosphate at 100nm magnification with particles sizes ~ 45 to 64nm in diameter, B) 24 hour synthesis of amorphous Al-phosphate zoomed out to 1 μ m, exhibiting aggregates of particles within clusters, C) 24 hour reacted amorphous Al-phosphate material magnified to 100nm, demonstrating particle sizes similar to those of the unreacted, but with slightly smaller diameters. D) Aggregate of unreacted amorphous Al-phosphate synthesized at 24 hours.

Appendix A, Figure 7- Micrographs of nanoporous amorphous Fe-phosphate taken by Field-Emission Scanning Electron Microscopy (FE-SEM), charging was present on material surfaces causing interference of images. A) and B) 24 hour synthesized amorphous Fe-phosphate at 100nm magnification with particles sizes ~ 26 to 100nm in diameter, C) 24 hour reacted amorphous Fe-phosphate material magnified to 100nm, demonstrating particle sizes similar to those of the unreacted, but slightly smaller diameters in some instances, aggregates of reacted material exhibit

potentially less porosity than unreacted material. D) Aggregate of unreacted amorphous Fe-phosphate synthesized at 24 hours.

Appendix A, Figure 8- X-ray Diffraction patterns of amorphous material. A) Synthesized amorphous Fe-phosphate and B) Synthesized amorphous Al-phosphate. Peaks at $\sim 45^\circ$ and 50° are from the aluminum stub which powered sample was mounted on.